General Psychiatry

Single-nucleus transcriptome profiling of prefrontal cortex induced by chronic methamphetamine treatment

Kuan Zeng,[1,2] Xuan Yu,[3] Zhen Wei,[3,4] Yong Wu,[1,2] Jianzhi Wang,[3,5] Rong Liu,[3] Yi Li [ID],[1,2] Xiaochuan Wang [ID] [3,5]

KZ, XY and ZW contributed equally.

For numbered affiliations see end of article.

Correspondence to
Dr Xiaochuan Wang; wxch@mails.tjmu.edu.cn

Dr Yi Li; psylee@163.com

ABSTRACT

Background Methamphetamine (METH) addiction causes a huge burden on society. The prefrontal cortex (PFC), associated with emotion and cognitive behaviours, is also involved in addiction neurocircuitry. Although bulk RNA sequencing has shown METH-induced gene alterations in the mouse PFC, the impact on different cell types remains unknown.

Aims To clarify the effects of METH treatment on different cell types of the PFC and the potential pathways involved in METH-related disorders.

Methods We performed single-nucleus RNA sequencing (snRNA-seq) to examine the transcriptomes of 20 465 nuclei isolated from the PFC of chronic METH-treated and control mice. Main cell types and differentially expressed genes (DEGs) were identified and confirmed by RNA fluorescence in situ hybridization(FISH).

Results Six main cell types were identified depending on the single-cell nucleus sequencing; of particular interest were the mature oligodendrocytes in the PFC. The DEGs of mature oligodendrocytes were enriched in the myelin sheath, adenosine triphosphate (ATP) metabolic process, mitochondrial function and components, and so on. The messenger RNA levels of *Aldoc* and *Atp5l* (FISH) and the protein level of the mitochondrial membrane pore subunit TOM40 (immunofluorescence) decreased in the mature oligodendrocytes. Fast blue staining and transmission electron microscopy image indicated myelin damage, and the myelin thickness decreased in METH brains.

Conclusions snRNA-seq reveals altered transcriptomes of different cell types in mouse PFC induced by chronic METH treatment, underscoring potential relationships with psychiatric disorders.

INTRODUCTION

Methamphetamine (METH) abuse has become a worldwide public problem, and the production, trafficking and consumption of METH have significantly increased in recent years.[1 2] METH is a powerful nervous system stimulant and highly addictive; its use results in both psychiatric and physical symptoms.[1 3 4] However, current therapies for METH use disorder, including psychotherapy and behavioural management, lack efficacy,

WHAT IS ALREADY KNOWN ON THIS TOPIC

⇒ Methamphetamine (METH) abuse is a worldwide public problem, but current therapies for METH use disorder remain unclear.
⇒ Chronic METH abuse alters various cell types in the brain and can cause cognitive decline and various psychiatric symptoms.
⇒ The mechanisms of METH-induced cell-specific gene transcriptional changes and METH psychosis require further research.

WHAT THIS STUDY ADDS

⇒ In this study, single-nucleus RNA sequencing was used to reveal the cell type-specific effects of chronic METH treatment on the mouse prefrontal cortex and identify potential pathways involved in METH-related disorders.

HOW THIS STUDY MIGHT AFFECT RESEARCH, PRACTICE OR POLICY

⇒ This study provides new insights into cell-specific gene transcriptional alterations in the prefrontal cortex of chronic METH-treated mice and gives hints for studying the mechanisms of METH-related disorders.

and the mechanisms underlying addiction remain unclear.[5 6]

Chronic METH abuse alters various cell types in the brain. METH activates dopamine, norepinephrine and serotonin receptors by binding their membrane-bound transporters[7] and releasing neurotransmitters, which is the foundation of the euphoric effects and addiction.[8] Chronic METH abuse also damages dopamine and serotonin nerve terminals by decreasing dopamine storage in the brain. A series of events, including oxidative stress, neurotoxic effects, excitatory neurotoxicity and neuroinflammation, happen after METH use,[7 9] and glia cells are altered. Daily METH-treated rats exhibit decreased neurogenesis and gliogenesis in the medial prefrontal cortex (PFC).[10] *In vitro* experiments previously revealed the cell type-specific transcription in

METH-treated organoids, with especially strong effects on cytokines and inflammasome-related genes and the robust transcriptional response of astrocytes.[11] METH induces cytotoxicity in rat oligodendrocytes by increasing the expression of proapoptotic proteins (bax and DP5).[12] Chronic METH treatment induces reactive microgliosis in the brains of both humans and animals.[13] However, the characteristics of the gene transcriptome affected in different cell types of METH-treated animals have not been investigated.

METH abuse can cause cognitive decline and various psychiatric symptoms, including irritability, anxiety, psychosis and mood disturbances.[3 14] Furthermore, psychiatric diseases such as schizophrenia,[15] affective disorders and antisocial personality disorder are also risk factors for METH psychosis.[16] Although epidemiology studies have revealed common phenotypes and complex associations between METH abuse and psychiatric diseases, the shared mechanisms of primary and METH-induced psychotic disorders still need further research.[17] As an essential brain region, the PFC is involved in higher-order functions of cognition, emotion, motivation, attention, and memory and planning.[18] Addiction-induced PFC abnormalities are associated with both compulsive drug-taking and negative addictive drug-related behaviours via regulation of limbic reward regions and higher-order executive function.[19 20] Chronic METH use can reduce dopamine transporter levels in the PFC, aggravating psychiatric symptoms.[21] METH abusers exhibit low PFC activation, consistent with their fundamental cognitive deficits during decision-making tasks.[22] METH also alters the messenger RNA (mRNA) levels of genes related to autophagy, apoptosis and inflammation, and brain-derived neurotrophic growth factor levels decrease in the PFC.[23] However, whether METH can induce PFC cell-specific gene transcriptional changes to promote METH psychosis requires further research.

As a revolutionary medical research tool, single-cell/nucleus RNA sequencing (RNA-seq) has recently been used to identify subtypes of brain cells and the altered transcriptional characteristics of different cell types in neurodegenerative and neuropsychiatric diseases.[24] Researchers also have used single-cell RNA-seq to describe unique transcriptional responses of different cell types to morphine, cocaine and alcohol.[25–27] In this study, single-nucleus RNA sequencing (snRNA-seq) was used to reveal the cell type-specific effects of chronic METH treatment on the mouse PFC and indicated the potential pathways involved in METH-related disorders.

MATERIALS AND METHODS
Animals and tissue collection
Animals included in the current study were all 2-month-old male C57BL/6 mice. All animals were socially housed on a 12-hour light/dark cycle with water and food ad libitum. Mice were treated with 5 mg/kg METH or saline (intraperitoneal) for 14 days in the METH and control groups, respectively.[28] Animals were assigned to each experimental group randomly using a random numbers table. Similarly, the order of animal treatment was determined randomly with the help of a random number generator that identified the cage number for initiating treatment each day. Then all mice were deeply anaesthetised with chloral hydrate and sacrificed, and the PFCs of three mice per group were rapidly removed and prepared for single-nucleus isolation on ice.[29] The flowchart of the experimental procedure is shown in figure 1.

Single-nucleus isolation and library preparation
Iodixanol gradient centrifugation was used for single-nucleus isolation.[30] Briefly, we prepared a fresh homogenisation buffer on ice. The tissue was transferred to Petri dishes and washed in cold phosphate-buffered saline (PBS). Then it was cut into small pieces (2–3 mm^3)
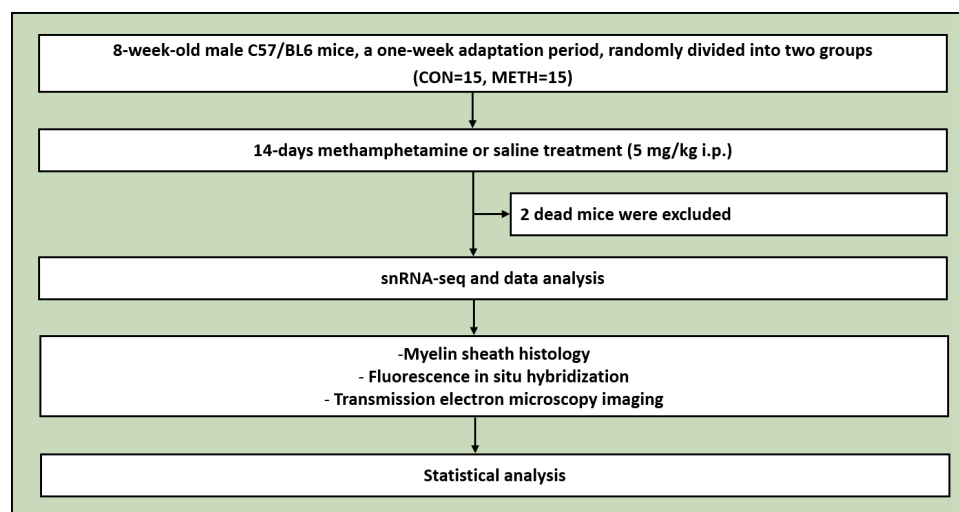
Figure 1 Flowchart of the study. CON, control; i.p., intraperitoneal injection; METH, methamphetamine; snRNA-seq, single-nucleus RNA sequencing.

and homogenised in 1.5 mL tubes, avoiding bubbles. Cold homogenisation buffer (0.7 mL) was added into each tube, gently mixed with samples and filtered by 40 μm cell filters. The mixture was centrifuged under 1000 g for 8 min (4 °C), and the sediment was suspended with a homogenisation buffer. Next, 50% iodixanol of the same volume was added to the buffer, and the mixture was then added to the 29% iodixanol 1:1. Nuclei were obtained after 13 500 g centrifugation for 20 min (4 °C). The precipitation was added with 1 mL PBS-bovine serum albumin (BSA) to suspend. The mixture was centrifuged again under 1000 g for 8 min (4 °C) and resuspended the nuclei with 200 μL PBS-BSA. Single nuclei were counted after attenuation and dyed with trypan blue in blood cell counting plates. A proper amount of single nuclei (~8000) was added to the reverse transcription mixture, single-cell 3′ gel beads (combined with 10× barcode) and partitioning oil in the 10× Genomics Chromium Single Cell Controller before starting the GEM (Gel Bead-In-EMulsions) generation programme. GEM generation, reverse transcription, complementary DNA (cDNA) amplification and library construction were performed followed by the standard protocols of 10× genomics. A library quality check was performed by Qubit and Agilent 2100 Bioanalyzer (Agilent Technologies, Santa Clara, California, USA). The concentration of the library was >5 ng/μL and the length was in the range of 300–400 bp. Finally, the library sequencing was performed in the Illumina Hiseq platform (Illumina, San Diego, California, USA) under the 2× 150 bp double-ended sequencing pattern to generate FastQ data. Raw data have already been submitted to GEO (GSE190800).[31]

Preprocessing of single-cell gene expression data

Raw reads were preprocessed by the cellranger software (V.1.3.0). Sequencing data of each sample were analysed using the count function of cellranger, and the sequencing data of different samples were identified by their barcodes. The sequencing data were aligned to reference genome sequence by mm10_premrna, and the expression levels of the genes in every nucleus were obtained. The batch effects between samples were eliminated by the aggr function of the cellranger software. Seurat software (V.4.2.0) was used for initial quality control with the following steps: (1) genes expressed in fewer than three cells were removed; (2) cells expressing less than 200 unique genes were removed; and (3) cells that expressed 400–4000 unique molecular identifiers were included in further analysis. The data were then normalised by NormalizeData function with LogNormalize method (scale factor 10 000).

Principal components analysis and t-distributed stochastic neighbour embedding plot

The average expression and standardised variance of genes in all cells were calculated by FindVariableFeatures of Seurat software (V.4.2.0). We selected 2000 variable genes for further analysis (online supplemental figure 1A). The data were preprocessed by the ScaleData function and processed for principal component analysis (PCA) with the RunPCA function. The principal component scores (p values) and standard deviation (SD) were calculated and visualised by JackStrawPlot and the ElbowPlot function, respectively (online supplemental figure 1B,C). Cells were clustered using the FindClusters function under the 0.5 resolution ratio. The t-distributed stochastic neighbour embedding (t-SNE) plots were generated with the RunTSNE function in Seurat software (V.4.2.0).

Cluster markers and DEG identification

Marker genes of clusters were identified among genes whose expression levels were significantly different compared with other clusters. These marker genes were generated with the FindAllMarkers function of Seurat software (gene expression cells/total cells >0.25, |log$_2$ foldchange| >2, q-value <0.05). Differentially expressed genes (DEGs) between the METH and control groups were identified by two-sided Wilcoxon tests in R package (gene expression cells/total cells >0.20, |log$_2$ foldchange| >0.4, q-value <0.05).

Functional enrichment analysis

Variable genes were identified using the FindMarkers function. Gene Ontology (GO) analysis was performed using the enrichGO function of clusterProfiler in R (V.4.4.4). Kyoto Encyclopedia of Genes and Genomes (KEGG) analysis was performed using the enrichKEGG function of clusterProfiler, and the parameters were set as follows: qvalueCutoff=0.05, pvalueCutoff=0.01.

Fluorescence in situ hybridization

Mice were perfused with ice-cold PBS followed by cardiac perfusion of ice-cold 4% paraformaldehyde (PFA) after sacrifice. The brains were obtained rapidly on ice and incubated in 4% PFA (4 °C) for 24 hours, then transferred to 10%, 20% and 30% sucrose solution in sequence for dehydration (4 °C). Frozen sections were cut at 20–30 μm under −20 °C. RNA fluorescence in situ hybridization (FISH) was performed according to the Enhanced Sensitive ISH Detection Kit protocol from Boster Biological Technology (Wuhan, China). The sections were washed with PBS at room temperature three times and then incubated with 0.5% Triton-PBS for 30 min. Every section was incubated with a prehybridization solution for 3 hours (38 °C–42 °C) in a box with 20% glycerinum at the bottom. Next, the prehybridization solution was removed, and sections were incubated with hybridization solution overnight (38 °C–42 °C). The sections were washed with 2× saline sodium citrate (SSC) (37 °C) for 15 min (twice), followed by 0.5× SSC, then 0.2× SSC for 15 min each in sequence. Sections were incubated with blocking solution for 30 min, biotinylation-mouse antidigoxin for 60 min (37 °C) and strept(avidin)-biotin complex-fluorescein isothiocyanate-PBS (SABC-FITC-PBS) for 30 min (37 °C). Sections were then blocked with 3% BSA-PBS for 1 hour.

The antibodies were diluted in PBS at 1:200 and used for section incubation overnight at 4 °C. The sections were washed with PBS and incubated with the secondary antibody for 2 hours at room temperature. The FISH slides were observed on a Zeiss LSM 780 confocal microscope (Zeiss, Oberkochen, Germany).

For mRNA quantification, images were acquired via a confocal microscope. First, the area of the PFC in the samples was determined using a 10× objective lens, and the objective lens was then changed to 20× and a picture was acquired. Fixed parameters were guaranteed without overexposure conditions and separated into three channels (red, blue and green) via ImageJ software (National Institutes of Health, Bethesda, Maryland, USA). First, circled red regions (myelin oligodendrocyte glycoprotein positive regions, which were abbreviated as MOG+) were identified as regions of interest (ROIs). Then the green channel which labelled the mRNA of target genes was loaded into the ROI to obtain the mean grey value. In each sample, 5–18 cells were counted and the average value was calculated; five samples were used in each group.

Myelin sheath histology

Frozen PFC sections (prepared as described in the Fluorescence in situ hybridization section) were stained by Luxol Fast Blue dye solution for 12 hours (room temperature), followed by 30 s in 70% alcohol and redyeing in eosin staining solution for 3 min. The sections were dehydrated, hyalinised by xylene and covered with neutral balsam. Luxol Fast Blue myelin sheath staining kits (Leagene, Beijing, China) were used according to the manufacturer's instructions. The myelin sheaths were aquamarine blue and the cell bodies were red.

Transmission electron microscopy imaging

Fresh PFC tissue was isolated and fixed immediately in 2.5% glutaraldehyde (Servicebio, Wuhan, China) and washed with 0.1 M phosphate buffer. Then the tissue was postfixed by 0.1 M osmic acid for 2 hours. After dehydration, they were embedded with epoxy resin (SPI 812) and acetone and polymerised in a 60°C oven for 48 hours. The slices (60–80 nm) were cut on an Ultracut microtome (Leica, Wetzlar, Germany). The sections were stained by uranyl acetate and lead citrate for 15 min each. The ultrastructures of myelin were visualised and imaged by transmission electron microscope (HITACHI, Tokyo, Japan).

G-ratio analysis

For calculating g-ratios, axons with a diameter >0.3 µm were used for quantitative analysis and equal to the ratio of the inner-to-outer diameter of a myelinated axon. A minimum of 10 myelinated axons were analysed per mouse at the level of the PFC and the mean value was counted. The g-ratios were statistically compared between genotypes and time points, using a t-test for average values per animal.

Antibodies and reagents

The primary antibodies and reagents employed in this study are described in online supplemental table 1.

Statistical analysis

Data were analysed using GraphPad Prism V.7.00 software (GraphPad, San Diego, California, USA). All results are expressed as mean and the standard error of the mean (SEM). Student's t-tests were used to identify significant differences between means. Differences were considered statistically significant at p<0.05.

RESULTS

### Unbiased snRNA-seq analysis identified distinct cell types in the mouse PFC

The PFC regions were isolated from six mice and dissociated into single nuclei. The raw data were generated after library preparation using the Illumina Hiseq platform (figure 2A). After quality control, transcriptomes of 20 465 nuclei (10 722 and 9743 from the control and METH groups, respectively) were obtained and included in the following analysis. To understand the effects of chronic METH treatment on cell-specific transcriptomes in PFC, the cells were assigned into 26 clusters through PCA (online supplemental figure A–C) and dimensionality reduction for two-dimensional visualisation of t-SNE[32] (figure 2B). Every cluster was detected in both groups. The ratios of cell numbers in most clusters were similar between the groups; however, the proportions of cluster oligodendrocytes 1 and total inhibitory neurons in the METH group increased, and the astrocytes, microglia and oligodendrocyte precursors cells (OPCs) decreased (online supplemental table 2). Expression of cell type-specific markers was used to identify those clusters: neuron (*Syt1+ Snap25+*), astrocytes (*Gja1+*), microglia (*P2ry12+*), oligodendrocyte (*Mag+*) and OPCs (*Pdgfra+*) (figure 2C,D).[33–35] Furthermore, neurons could be further identified as excitatory (*Satb2+*, *Lmo4+*) and inhibitory (*Gad2+*, *Gad1+*) neurons (figure 2C,D). The genes expressed differently in each cell type were calculated, and the results showed that all the main cell types exhibited METH-dependent alterations (figure 3A,B, online supplemental table 3).

Genes related to mitochondrial function and components were inhibited in PFC mature oligodendrocytes from METH mice

Both *in vitro* and *in vivo* experiments have shown oligodendrocyte damage following METH treatment.[10 12] Transcriptional alterations of oligodendrocytes induced by other addiction substances, such as alcohol and morphine, also have attracted attention.[25 26] Meanwhile, we also observed a unique effect of METH on PFC mature oligodendrocyte transcription profiles. All of clusters 0, 20 and 21 were identified as mature oligodendrocytes (*Mag+*) (figure 2C,D). The oligodendrocytes and inhibitory neurons have the largest numbers of downregulated genes in the METH group, and oligodendrocytes have the
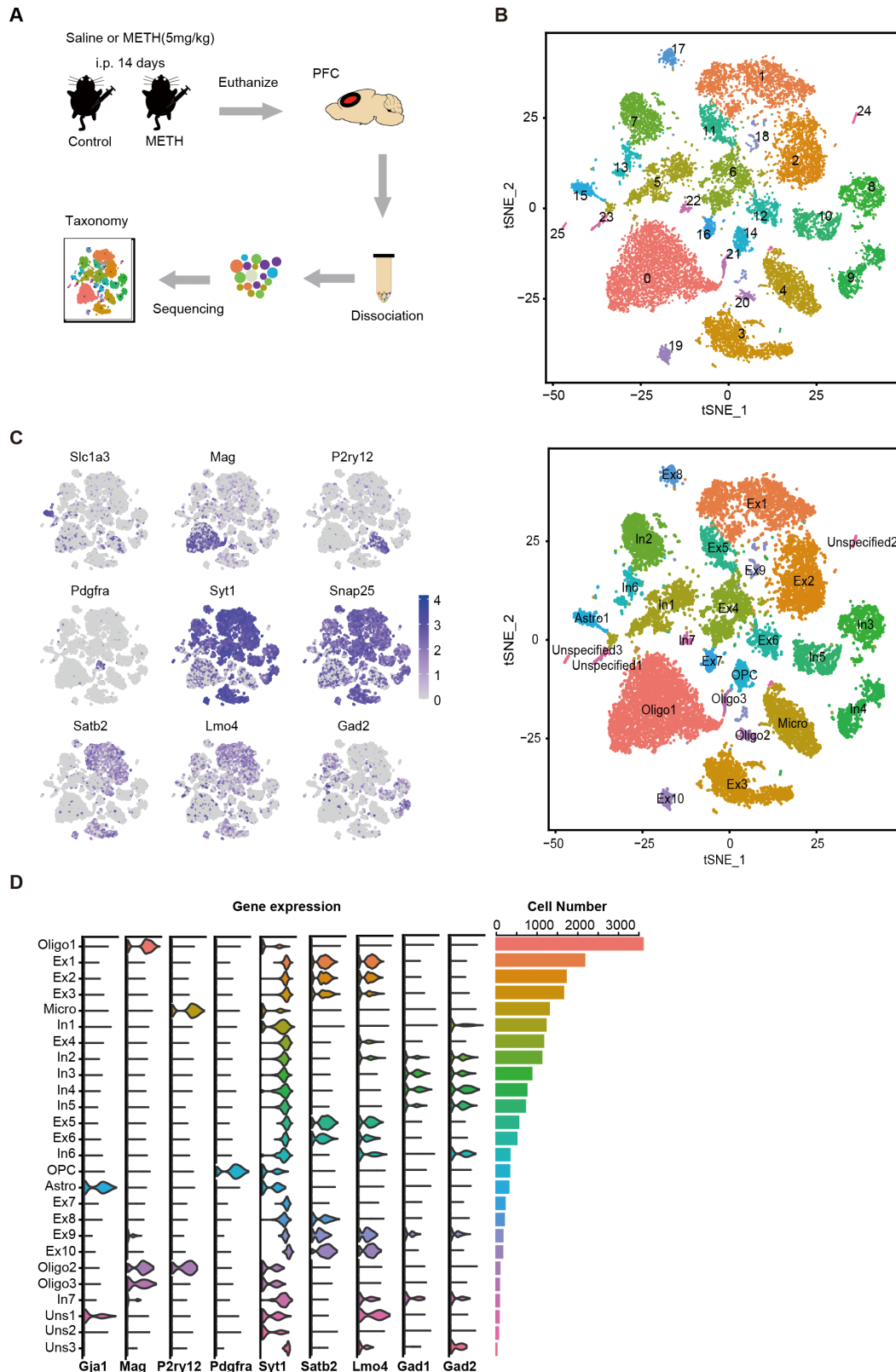
Figure 2 Single-nucleus RNA-seq-based cell type identification of mice PFC. (A) Flowchart of the snRNA-seq experimental design. (B) Two-dimensional visualisation t-SNE plot of snRNA-seq from six mice PFC (METH and control groups, n=3 each). There were 20 465 nuclei, which were divided into 26 clusters by PCA. Each colour represents one cluster. (C) Clusters in (B) were identified as seven cell types based on the expression of cell type-specific markers. The expression of every cell type-specific marker in the cluster is highlighted in blue (left). Expression of all cell type-specific markers in the clusters is highlighted in different colours (right). (D) Violin plot shows the expression of specific markers for all the clusters. METH, methamphetamine; PCA, principal components analysis; PFC, prefrontal cortex; snRNA-seq, single-nucleus RNA sequencing; t-SNE, t-distributed stochastic neighbour embedding.
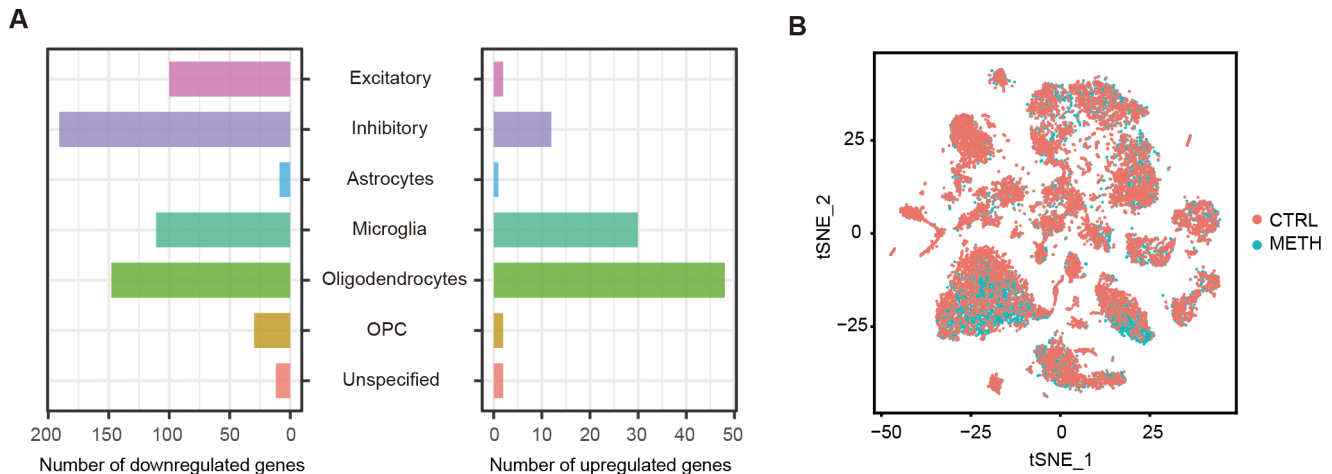
Figure 3 METH-induced cell type-specific gene transcription alterations. (A) DEGs of each PFC cell type between METH and control groups were selected with the FindAllMarkers function in Seurat software (gene expression cells/total cells >0.20, |log₂ foldchange| >0.4, q-value <0.05). The total numbers of unique genes significantly induced or reduced by METH are shown, grouped by major CNS cell type. (B) Two-dimensional visualisation t-SNE plot of snRNA-seq from the METH and control groups. Each colour represents one group. CNS, central nervous system; CTRL, control; DEGs, differentially expressed genes; METH, methamphetamine; OPC, oligodendrocyte precursors cell; PFC, prefrontal cortex; snRNA-seq, single-nucleus RNA sequencing; t-SNE, t-distributed stochastic neighbour embedding.

largest numbers of upregulated genes (figure 3A). The DEGs of mature oligodendrocytes between the METH and control groups were identified (online supplemental table 3). GO analysis revealed that genes altered in the METH group were mainly enriched in the mitochondrial membrane part, cytochrome complex, myelin sheath (cellular component) and adenosine triphosphate (ATP) metabolic process, and oxidative phosphorylation (biological process) (figure 4A, online supplemental table 4). KEGG analysis also indicated that downregulated genes in the METH group were enriched in oxidative phosphorylation pathways (figure 4B, online supplemental table 4). The expression levels of *Aldoc* (aldolase C) and cytochrome c oxidase subunits 6A1, 7A2, 5B, etc were significantly lower in the METH group than in the control group (figure 4C, online supplemental table 3).

METH also inhibited genes such as *Uqcrh* (ubiquinol-cytochrome c reductase hinge protein), *Uqcrq* (ubiquinol-cytochrome c reductase), and ATP synthase subunits 5l, 5b, etc, which were enriched in the ATP metabolic process pathway (figure 4D, online supplemental table 3). Thus, METH inhibits both mitochondrial components and the organelle's vital physiological functions in mice PFC oligodendrocytes. METH-induced altered genes also enriched in the myelin sheath, which is one of the most important functions of mature oligodendrocytes; thus, related genes were also assessed. The mRNA levels of 17 genes enriched in myelin sheathes decreased in the METH group, including calmodulin genes (*Calm1*, *Calm2*, *Calm3*) (figure 4E, online supplemental table 3). Microglial activation and inflammation always accompany METH-induced neurotoxicity.[36 37] We also found DEGs of microglia that were upregulated in the METH group were enriched in tumour necrosis factor production (*Cyba*, *Fcgr3*,

Pik3r1, *Arrb2*), leucocyte-mediated cytotoxicity (*Ctsh*, *Lag3*) and heat shock protein binding (*Fkbp5*, *Mettl23*) (online supplemental table 5). These results indicate that METH may induce PFC microglia production of inflammatory mediators.

In vivo validation of oligodendrocyte-specific genes and mitochondria alteration in the PFC of METH mice

FISH was performed to validate differences in mRNA levels in PFC-specific cells between the two groups. The DEGs (gene expression cells/total cells>0.20, foldchange>2, both p<0.001) of mature oligodendrocytes related to the ATP metabolic process (*Aldoc* and *Atp5l*) were selected, and the mRNAs were labelled by FISH and merged with mature oligodendrocytes and myelin marker *Mog* (figure 5A,C). The mRNA levels of *Aldoc* and *Atp5l* significantly decreased in PFC oligodendrocytes of METH mice, mirroring the snRNA-seq results (figure 5B,D). Although *Tomm40* mRNA levels were not significantly different between the METH and control groups (p>0.05), protein levels of the mitochondrial membrane pore subunit TOM40 decreased in PFC oligodendrocytes from METH mice (figure 5E,F), indicating that altered cellular component pathways of mitochondrial membrane partly may affect the number of mitochondria.[38] Although the myelin genes did not show significant differences, there was a marked loss of myelin sheaths in the PFC of METH mice (figure 6A). Transmission electron microscopy confirmed myelin sheath damage (lamellae separation and integrity deficits) in METH mice (figure 6B). The g-ratio of the METH group significantly increased, indicating that myelin thickness was decreased in METH-treated mice (figure 6C).
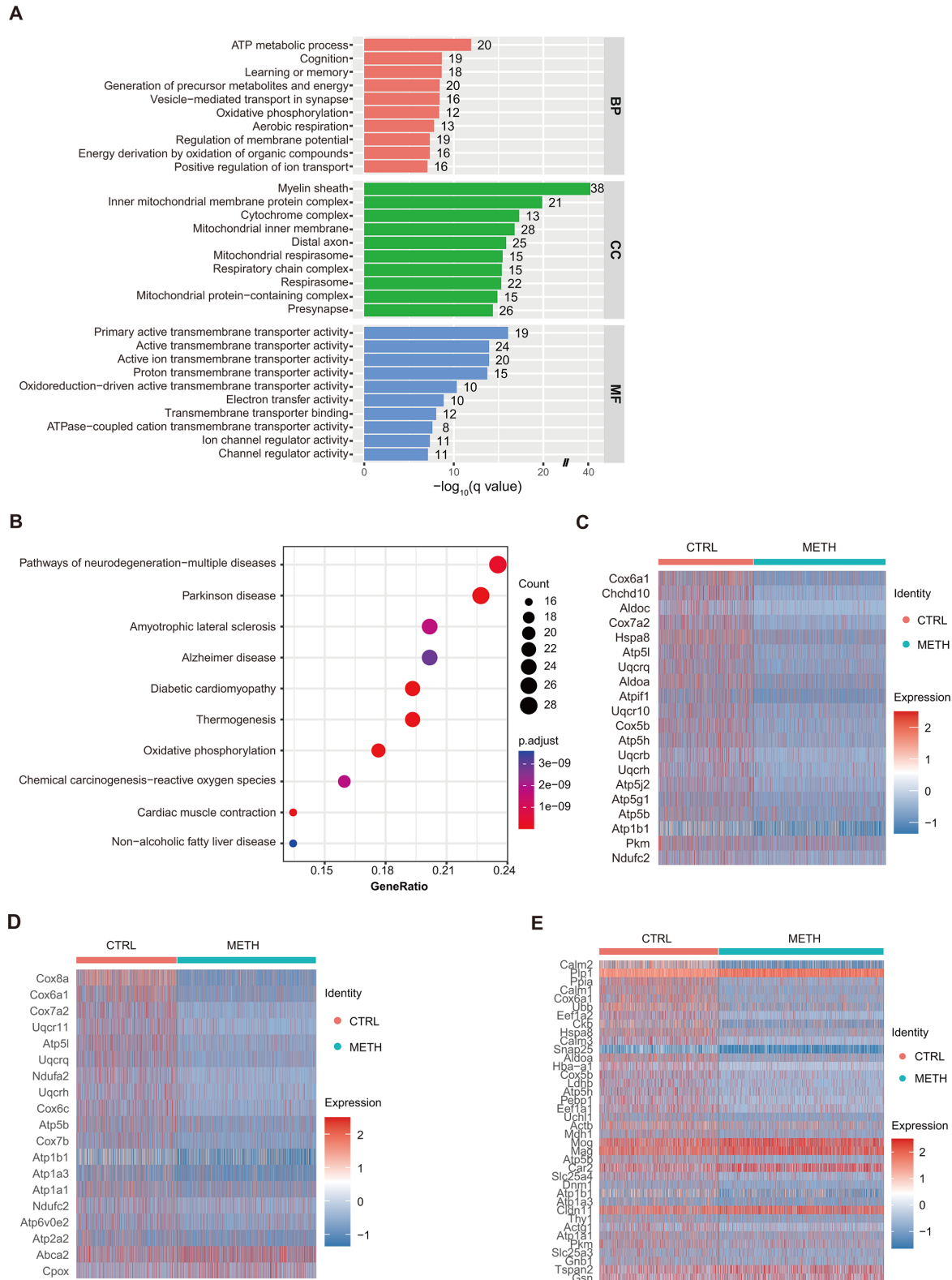
Figure 4 Characteristics of PFC mature oligodendrocytes DEGs between METH and control groups. (A) GO analysis showing the top 30 pathways (BP, CC and MF were 10 each, respectively) derived from the DEGs. DEGs between the METH and control groups, gene expression cells/total cells>0.20, |log$_2$ foldchange|>0.4, two-sided Wilcoxon test, p<0.01. (B) KEGG analysis revealed DEGs related to neurodegenerative diseases (Parkinson's disease, Alzheimer's disease and Huntington's disease) and oxidative phosphorylation. (C) Heatmap of DEGs enriched in the oxidative phosphorylation pathway. (D) Heatmap of DEGs enriched in the ATP metabolic process pathway. (E) Heatmap of DEGs enriched in the myelin sheath pathway. ATP, adenosine triphosphate; BP, biological process; CC, cellular component; CTRL, control; DEGs, differentially expressed genes; GO, Gene Ontology; KEGG, Kyoto Encyclopedia of Genes and Genomes; METH, methamphetamine; MF, molecular function; PFC, prefrontal cortex.
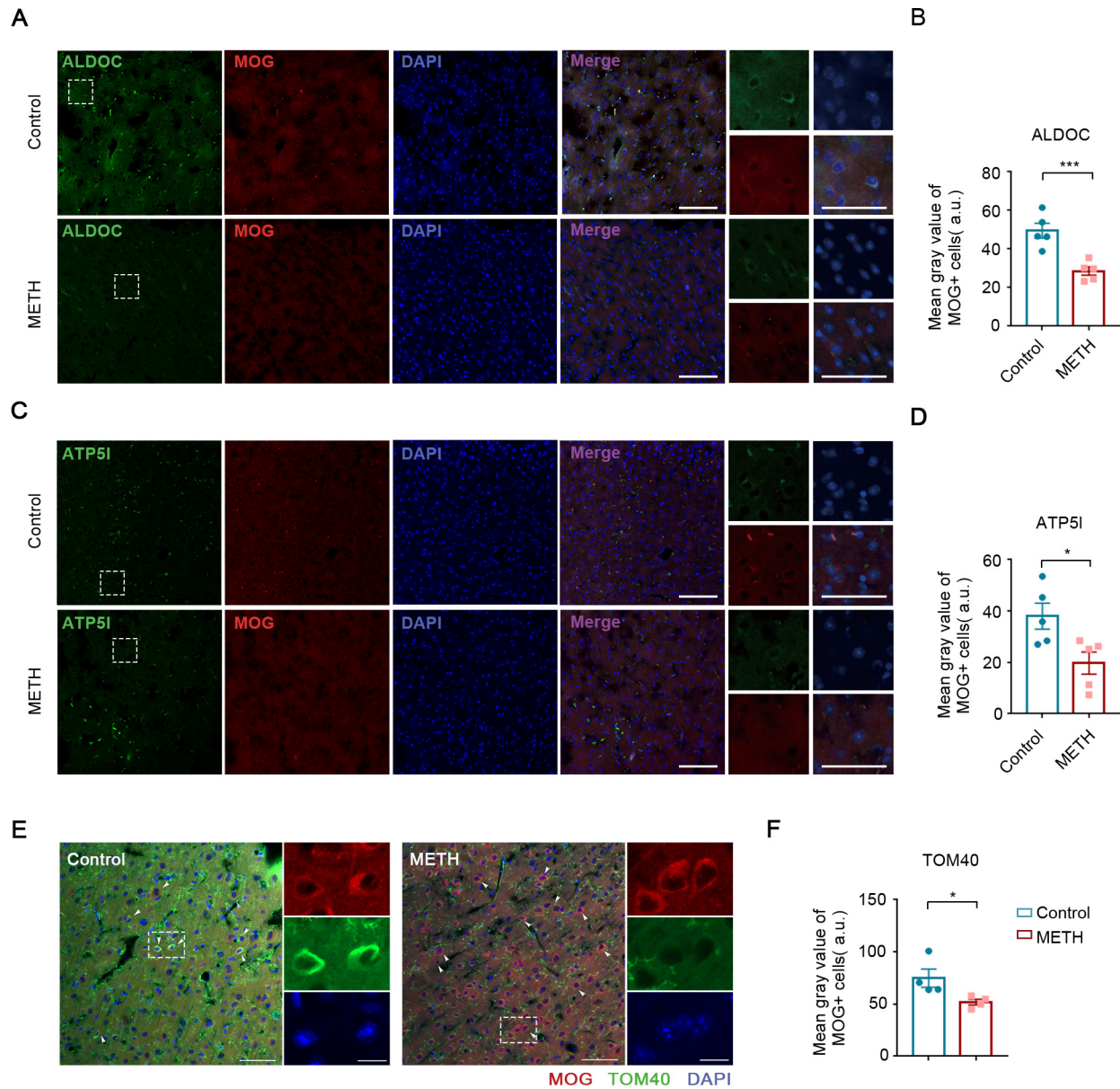
Figure 5 *In vivo* validation of oligodendrocyte-specific genes and mitochondria altered in the PFC of METH-treated mice. (A) FISH detection of *Aldoc* mRNA (green) in oligodendrocytes (MOG antibody labelled, red) in the mouse PFC. Nuclei were stained with DAPI (blue). Scale bars, 100 μm (inset, 50 μm). (B) Statistical analysis of (A). Quantification of *Aldoc*+ MOG+ cells in different mice (METH group, n=5; control group, n=5) at 20×. Two-sided Student's t-test, ***p=0.002 (F-test to compare variances: p=0.308). (C) FISH detection of *Atp5l* mRNA (green) in oligodendrocytes (MOG antibody labelled, red) in the mouse PFC. Nuclei were stained with DAPI (blue). Scale bars, 100 μm (inset, 50 μm). (D)Statistical analysis of (C). Quantification of *Atp5l*+ MOG+ cells in different mice (METH group, n=5; control group, n=5) at 20×. Student's t-test, two-sided, *p=0.025 (F-test to compare variances: p=0.767). (E) Fluorescence-detected mitochondria (TOM40 antibody labelled, green) of oligodendrocytes (MOG antibody labelled, red) in mice PFC. The nucleus was stained by DAPI (blue). Scale bars, 50 μm. (F) Statistical analysis of (E). Quantification of TOM40+ MOG+ cells in four mice (each group) at 20×. Student's t-test, two-sided, *p=0.048 (F-test to compare variances: p=0.086). a.u., arbitrary units; DAPI, 4′,6-diamidino-2-phenylindole; FISH, fluorescence in situ hybridization; METH, methamphetamine; MOG, myelin oligodendrocyte glycoprotein; mRNA, messenger RNA; PFC, prefrontal cortex.

DISCUSSION
Main findings

In this research, we used snRNA-seq to identify PFC cell types in chronic METH-treated mice and control mice. By identifying the main cell types in PFC and calculating DEGs via Serut software (figure 2C), we identified obvious METH-induced gene transcriptional alterations. The main cell types of PFC were found in our results; however, three clusters (clusters 23, 24 and 25) containing small numbers of cells could not be identified by only the classic gene markers (figure 2C).

With the development of single cell/nucleus RNA-seq, transcriptomes of non-neuronal cells in the brain are no longer overlooked in substance addiction research. As one of the main cell types in the brain, oligodendrocytes generate myelin and support axonal functions
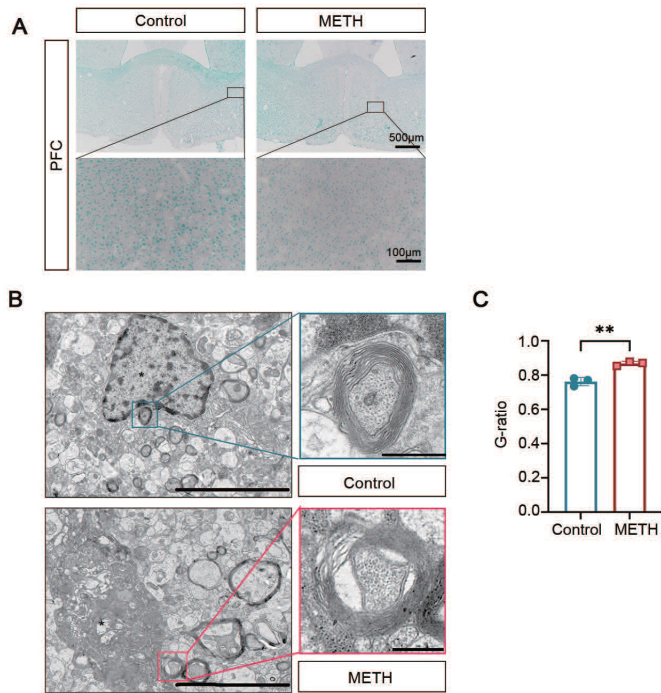
Figure 6 METH-induced myelin damage in mice PFC. (A) Representative images of Luxol Fast Blue staining kit labelling of the myelin sheath in mice PFC from METH and control groups. Scale bars, 50 µm. Aquamarine blue represents myelin sheaths, and red represents cell bodies. (B) Representative images of myelin sheaths structure in mice PFC from METH and control groups under transmission electron microscopy. Scale bars, 5 µm (left), 500 nm (right). (C) G-ratio of myelinated axons. Significant increases in the g-ratio were measured in METH mice (n=3 animals per age group) compared with wild-type control. Data represent mean±SEM, and p value significance is calculated from an unpaired two-tailed Student's t-test, **p=0.003 (F-test to compare variances: p=0.439). METH, methamphetamine; PFC, prefrontal cortex. SEM, standard error of the mean.

and are therefore indispensable for maintaining nerve conduction.[39] In the human alcoholic brain, there were more DEGs in astrocytes, oligodendrocytes and microglia compared with neurons.[27] Similarly, morphine induces unique transcriptional responses of oligodendrocytes and astrocytes in mice.[25]

Oligodendrocytes play an essential role in neuronal metabolism and provide neuronal metabolic support through monocarboxylate transporters,[40] which could also be involved in major mental disorders, including schizophrenia, bipolar and major depressive disorders, alcoholism, and cocaine addiction.[41] Depending on our sn-RNAseq analysis, METH treatment significantly affects METH on oligodendrocytes' mitochondrial functions and myelin sheath generation. Thus, we hypothesise that the alterations of metabolic and myelin-related genes on the transcriptional level of mature oligodendrocytes might be the early promoting factors in the progression of METH-related disorders. In this research, different mature oligodendrocyte transcriptional characteristics between METH and control mice attracted attention (figure 3B).

Specifically, genes related to mitochondrial components and functions were significantly downregulated in PFC mature oligodendrocytes in the METH group (figures 3 and 4). Morphological imaging confirmed mitochondrial damage and loss (figure 5), as well as severe myelin damage and loss in METH brains (figure 6).

Oligodendrocytes are highly sensitive to energy deprivation, such as ischaemia.[42 43] However, reducing the mitochondrial functions of oligodendrocytes by disturbing cytochrome c oxidase does not typically cause demyelination or axonal degeneration in adult mice.[44] It is hard to determine the causal relationships and sequential order of oligodendrocyte mitochondrial abnormalities and myelin deficits in METH mice, but performing the experiments on mitochondrial functions in oligodendrocytes and the histology of myelin sheath may help address this issue.

Almost 40% of individuals who abuse METH suffer from psychotic symptoms and syndromes, creating a heavy burden for both patients and society.[17 45] Chronic METH psychosis has several common phenotypes with both negative/positive symptoms[46 47] and cognitive symptoms of schizophrenia.[48] METH dependence also increases the risk of bipolar disorder.[16] Current evidence indicates that long-term METH abuse can cause brain neuronal loss and atrophy, triggering cognitive impairments and premature ageing.[7 49] However, the mechanisms of METH-related disorders and the involvement of different cell types in these disorders are still unclear. GO and KEGG analyses of DEGs in different cell types induced by METH are helpful in finding pathways that are associated with these psychiatric diseases (online supplemental tables 3 and 5).

Limitations

Our results should also be considered in the context of several limitations, which need both bioinformatics and experimental verification. First, the subpopulations of the main PFC cell types need additional identification. Although classic gene markers could identify most of the clusters, the subtypes (especially neuron subtypes) could be further separated and confirmed by FISH. Second, our research mainly verified that the mitochondria-related genes of oligodendrocytes were altered at the transcription level; it remains unclear whether METH could induce mitochondrial dysfunction in oligodendrocytes, and the mechanisms should be explored. Lastly, to delineate the common mechanisms of METH addiction and psychiatric disorders at the cell-type transcriptome level, it would be useful to combine the results of single-cell/nucleus RNA-seq of samples from disease models with METH samples.[13]

Implications

Our snRNA-seq findings provide clues for cell type-specific gene transcriptional alterations in the PFC of chronic METH-treated mice and underscore potential pathways involved in METH-related disorders. The DEGs of PFC between METH-treated mice and control mice from all

the cell types were detected. Moreover, the specific effects of METH on the transcriptomes of mature oligodendrocytes should be given particular attention in future studies related to METH use, especially the functions related to metabolic pathways and mitochondrial functions.

Author affiliations
[1]Department of Psychiatry, Wuhan Mental Health Center, Wuhan, Hubei, China
[2]Research Center for Psychological and Health Sciences, China University of Geosciences, Wuhan, Hubei, China
[3]Department of Pathophysiology, School of Basic Medicine, Key Laboratory of Education Ministry/Hubei Province of China for Neurological Disorders, Huazhong University of Science and Technology Tongji Medical College, Wuhan, Hubei, China
[4]Department of Pathology, Maternal and Child Hospital of Hubei Province, Huazhong University of Science and Technology Tongji Medical College, Wuhan, Hubei, China
[5]Co-innovation Center of Neuroregeneration, Nantong University, Nantong, Jiangsu, China

ORCID iDs
Yi Li http://orcid.org/0000-0002-8876-0041
Xiaochuan Wang http://orcid.org/0000-0001-8207-0042

REFERENCES
1 Paulus MP, Stewart JL. Clinical presentation, and treatment of methamphetamine use disorder: a review. *JAMA Psychiatry* 2020;77:959–66.
2 Piper BJ, Ogden CL, Simoyan OM, *et al*. Trends in use of prescription stimulants in the United States and territories, 2006 to 2016. *PLoS One* 2018;13:e0206100.
3 Zweben JE, Cohen JB, Christian D, *et al*. Psychiatric symptoms in methamphetamine users. *Am J Addict* 2004;13:181–90.
4 Darke S, Kaye S, McKetin R, *et al*. Major physical and psychological harms of methamphetamine use. *Drug Alcohol Rev* 2008;27:253–62.
5 Dutra L, Stathopoulou G, Basden SL, *et al*. A meta-analytic review of psychosocial interventions for substance use disorders. *Am J Psychiatry* 2008;165:179–87.
6 Ballester J, Valentine G, Sofuoglu M. Pharmacological treatments for methamphetamine addiction: current status and future directions. *Expert Rev Clin Pharmacol* 2017;10:305–14.
7 Sulzer D, Sonders MS, Poulsen NW, *et al*. Mechanisms of neurotransmitter release by amphetamines: a review. *Prog Neurobiol* 2005;75:406–33.
8 Prakash MD, Tangalakis K, Antonipillai J, *et al*. Methamphetamine: effects on the brain, gut and immune system. *Pharmacol Res* 2017;120:60–7.
9 Yang X, Wang Y, Li Q, *et al*. The main molecular mechanisms underlying methamphetamine- induced neurotoxicity and implications for pharmacological treatment. *Front Mol Neurosci* 2018;11:186.
10 Mandyam CD, Wee S, Eisch AJ, *et al*. Methamphetamine self-administration and voluntary exercise have opposing effects on medial prefrontal cortex gliogenesis. *J Neurosci* 2007;27:11442–50.
11 Dang J, Tiwari SK, Agrawal K, *et al*. Glial cell diversity and methamphetamine-induced neuroinflammation in human cerebral organoids. *Mol Psychiatry* 2021;26:1194–207.
12 Genc K, Genc S, Kizildag S, *et al*. Methamphetamine induces oligodendroglial cell death in vitro. *Brain Res* 2003;982:125–30.
13 Sekine Y, Ouchi Y, Sugihara G, *et al*. Methamphetamine causes microglial activation in the brains of human abusers. *J Neurosci* 2008;28:5756–61.
14 Dean AC, Groman SM, Morales AM, *et al*. An evaluation of the evidence that methamphetamine abuse causes cognitive decline in humans. *Neuropsychopharmacology* 2013;38:259–74.
15 McKetin R, Hickey K, Devlin K, *et al*. The risk of psychotic symptoms associated with recreational methamphetamine use. *Drug Alcohol Rev* 2010;29:358–63.
16 Sulaiman AH, Said MA, Habil MH, *et al*. The risk and associated factors of methamphetamine psychosis in methamphetamine-dependent patients in Malaysia. *Compr Psychiatry* 2014:S89–94.
17 Glasner-Edwards S, Mooney LJ. Methamphetamine psychosis: epidemiology and management. *CNS Drugs* 2014;28:1115–26.
18 Kalin NH. Prefrontal cortical and limbic circuit alterations in psychopathology. *Am J Psychiatry* 2019;176:971–3.
19 Goldstein RZ, Volkow ND. Dysfunction of the prefrontal cortex in addiction: neuroimaging findings and clinical implications. *Nat Rev Neurosci* 2011;12:652–69.
20 Mistler CB, Shrestha R, Gunstad J, *et al*. Adapting behavioural interventions to compensate for cognitive dysfunction in persons with opioid use disorder. *Gen Psychiatr* 2021;34:e100412.
21 Sekine Y, Minabe Y, Ouchi Y, *et al*. Association of dopamine transporter loss in the orbitofrontal and dorsolateral prefrontal cortices with methamphetamine-related psychiatric symptoms. *Am J Psychiatry* 2003;160:1699–701.
22 Paulus MP, Hozack NE, Zauscher BE, *et al*. Behavioral and functional neuroimaging evidence for prefrontal dysfunction in methamphetamine-dependent subjects. *Neuropsychopharmacology* 2002;26:53–63.
23 Tehrani AM, Boroujeni ME, Aliaghaei A, *et al*. Methamphetamine induces neurotoxicity-associated pathways and stereological changes in prefrontal cortex. *Neurosci Lett* 2019;712:134478.
24 Skene NG, Bryois J, Bakken TE, *et al*. Genetic identification of brain cell types underlying schizophrenia. *Nat Genet* 2018;50:825–33.
25 Avey D, Sankararaman S, Yim AKY, *et al*. Single-cell RNA-Seq uncovers a robust transcriptional response to morphine by Glia. *Cell Rep* 2018;24:3619–29.
26 Bhattacherjee A, Djekidel MN, Chen R, *et al*. Cell type-specific transcriptional programs in mouse prefrontal cortex during adolescence and addiction. *Nat Commun* 2019;10:4169.
27 Brenner E, Tiwari GR, Kapoor M, *et al*. Single cell transcriptome profiling of the human alcohol-dependent brain. *Hum Mol Genet* 2020;29:1144–53.
28 Wang L, Qu G, Dong X, *et al*. Long-term effects of methamphetamine exposure in adolescent mice on the future ovarian reserve in adulthood. *Toxicol Lett* 2016;242:1–8.
29 Wang Q, Ding S-L, Li Y, *et al*. The Allen Mouse brain common coordinate framework: a 3d reference Atlas. *Cell* 2020;181:936–53.

30 MacArthur J, Bowler E, Cerezo M, *et al*. The new NHGRI-EBI catalog of published genome-wide association studies (GWAS catalog). *Nucleic Acids Res* 2017;45:D896–901.

31 Zeng K, Yu X, Wei Z, *et al*. Single nucleus RNA-Seq of Prefrontal cortex from methamphetamine-treated mice and control mice. 2021. Available: https://www.ncbi.nlm.nih.gov/geo/query/acc.cgi?acc=GSE190800 [Accessed 16 Feb 2023].

32 Kobak D, Berens P. The art of using t-SNE for single-cell transcriptomics. *Nat Commun* 2019;10:5416.

33 Zeisel A, Muñoz-Manchado AB, Codeluppi S, *et al*. Brain structure. cell types in the mouse cortex and hippocampus revealed by single-cell RNA-Seq. *Science* 2015;347:1138–42.

34 Zhong S, Zhang S, Fan X, *et al*. A single-cell RNA-Seq survey of the developmental landscape of the human prefrontal cortex. *Nature* 2018;555:524–8.

35 Tasic B, Yao Z, Graybuck LT, *et al*. Shared and distinct transcriptomic cell types across neocortical areas. *Nature* 2018;563:72–8.

36 Thomas DM, Walker PD, Benjamins JA, *et al*. Methamphetamine neurotoxicity in dopamine nerve endings of the striatum is associated with microglial activation. *J Pharmacol Exp Ther* 2004;311:1–7.

37 Hashimoto K, Tsukada H, Nishiyama S, *et al*. Protective effects of minocycline on the reduction of dopamine transporters in the striatum after administration of methamphetamine: a positron emission tomography study in conscious monkeys. *Biol Psychiatry* 2007;61:577–81.

38 Choong C-J, Okuno T, Ikenaka K, *et al*. Alternative mitochondrial quality control mediated by extracellular release. *Autophagy* 2021;17:2962–74.

39 Saab AS, Tzvetanova ID, Nave K-A. The role of myelin and oligodendrocytes in axonal energy metabolism. *Curr Opin Neurobiol* 2013;23:1065–72.

40 Philips T, Rothstein JD. Oligodendroglia: metabolic supporters of neurons. *J Clin Invest* 2017;127:3271–80.

41 Sokolov BP. Oligodendroglial abnormalities in schizophrenia, mood disorders and substance abuse. Comorbidity, shared traits, or molecular phenocopies? *Int J Neuropsychopharmacol* 2007;10:547–55.

42 Petito CK, Olarte JP, Roberts B, *et al*. Selective glial vulnerability following transient global ischemia in rat brain. *J Neuropathol Exp Neurol* 1998;57:231–8.

43 Dewar D, Underhill SM, Goldberg MP. Oligodendrocytes and ischemic brain injury. *J Cereb Blood Flow Metab* 2003;23:263–74.

44 Fünfschilling U, Supplie LM, Mahad D, *et al*. Glycolytic oligodendrocytes maintain myelin and long-term axonal integrity. *Nature* 2012;485:517–21.

45 Courtney KE, Ray LA. Methamphetamine: an update on epidemiology, pharmacology, clinical phenomenology, and treatment literature. *Drug Alcohol Depend* 2014;143:11–21.

46 Tomiyama G. Chronic schizophrenia-like states in methamphetamine psychosis. *Jpn J Psychiatry Neurol* 1990;44:531–9.

47 Wang L-J, Lin S-K, Chen Y-C, *et al*. Differences in clinical features of methamphetamine users with persistent psychosis and patients with schizophrenia. *Psychopathology* 2016;49:108–15.

48 Yamamuro K, Makinodan M, Kimoto S, *et al*. Differential patterns of blood oxygenation in the prefrontal cortex between patients with methamphetamine-induced psychosis and schizophrenia. *Sci Rep* 2015;5:12107.

49 Thompson PM, Hayashi KM, Simon SL, *et al*. Structural abnormalities in the brains of human subjects who use methamphetamine. *J Neurosci* 2004;24:6028–36.

Kuan Zeng is currently a researcher at the Wuhan Mental Health Center in China. He got his PhD at Tongji Medical College, Huazhong University of Science and Technology, China in 2017. He started working at the Wuhan Mental Health Center the same year as a research assistant. Currently, he is the deputy director of the science and education department. He has principally studied the pathogenesis and molecular mechanisms of neurodegenerative diseases and psychiatric conditions, such as Alzheimer's disease and depression. In addition, he is passionate about studying methamphetamine abuse.

Xuan Yu obtained her bachelor's degree in preventive medicine from Tongji Medical College, Huazhong University of Science and Technology, China in 2018. She also completed her master's degree there in 2021. During this time, she participated in several research projects under the Key Laboratory of Education Ministry/Hubei Province of China for Neurological Disorder. In 2021 she also worked as a research student at the Max Planck Institute. Her main research interests include understanding the causes and development of neurodegenerative diseases and addiction.

Zhen Wei obtained a PhD degree from Tongji Medical College, Huazhong University of Science and Technology, China in 2022. She is currently working as a medical technician in the Department of Pathology at the Maternal and Child Hospital of Hubei Province in China. Her main research interests include basic research of neurodegenerative disorders, such as Alzheimer's disease (AD), PTSD, etc., and she has carried out a series of studies on the aetiology, pathogenesis, and prevention strategies of AD. She has also been an author on peer-reviewed papers published in Cell Death and Disease, Aging-US.